Experimental Mechanics
https://doi.org/10.1007/s11340-026-01348-5

SP ISS: MECHANICS OF SOFT AND LIVING MATTER

Ultrasound-Mediated Nanoparticle Selectivity in Stretchable Hydrogels

C. Ye[1] · T. H. Wong[1] · Y. Zheng[2] · R. Lu[2] · J. Ma[1] · S. Lin[1,3]

Received: 6 March 2026 / Accepted: 5 June 2026
© The Author(s) 2026

Abstract

Background Selective diffusion of different types of particles is desirable in multiple modern chemical and biological technologies. However, distinguishing the transport of particles with similar physical, chemical, or geometrical properties is challenging because their transport behavior is governed by nearly identical thermodynamic and kinetic conditions within the host medium.

Objective Existing efforts to achieve the selective diffusion of particles include size filtration by the mesh of polymeric networks or by specific chemical interactions through dynamic bonds. However, these approaches rely on pronounced differences in particle size or affinity. This study aims to explore ultrasound excitation as an engineering space to enhance nanoparticle selectivity through dynamic control of mechano-diffusion in polymer networks.

Methods We developed an ultrasound diffusion characterization platform (UDCP) to systematically observe and analyze the diffusion behavior of particles. By leveraging a model particle-hydrogel system and the ultrasound excitation, we generated tunable acoustic fields that impose cyclic mechanical perturbations on the polymer network and the embedded particles.

Results Through the UDCP, we characterized the diffusion of various molecules with different sizes under various stretches of the hydrogel media and different ultrasonic power levels. For the individual kind of particles, the low- and intermediate-power ultrasonic stimulations can enhance the diffusion across all sizes, while the high-power ultrasound can induce a non-monotonic trend of diffusion profile due to polymer network damage. For two types of particles, ultrasonic stimulation can enable strong particle diffusion selectivity under moderate power levels.

Conclusion Ultrasound stimulations amplify the particle diffusion selectivity in a non-invasive approach, which can be utilized as an ideal method to achieve the selective diffusion of broad classes of particles, forming universal applications of ultrasound in drug delivery, chemical remediation, and in-situ biosensing.

Keywords Particle diffusion · Selective transport · Ultrasound · Hydrogel · Mechano-diffusion

Introduction

Nanoparticle selectivity, the preferential transport of specific particles over others within a shared medium [1], is highly desirable in diverse modern technologies and numerous applications, including targeted drug delivery [2, 3], environmental remediation [4, 5], molecular separation [6, 7], 3D printing [8–10], strong bio-adhesives [11, 12], and in-situ biosensing [13–16]. Despite the broad applications and significance, it is challenging to achieve precise control over the selective diffusion of particles with similar physical, chemical, or geometrical properties under nearly identical thermodynamic and kinetic conditions within the host medium [1, 17–19].

C. Ye, T.H. Wong, Y. Zheng and R. Lu contributed equally to this work.

✉ T. H. Wong
tszwong@msu.edu

✉ S. Lin
linshaot@msu.edu

[1] Department of Mechanical Engineering, Michigan State University, East Lansing, MI, USA

[2] Department of Chemical Engineering and Materials Science, Michigan State University, East Lansing, MI, USA

[3] Department of Mechanical Engineering, University of Wisconsin-Madison, Madison, WI, USA

Published online: 05 August 2026

Existing efforts for achieving selective diffusion primarily rely on tailoring the structural or chemical properties of the diffusion medium. One common approach is to engineer the polymer network mesh size to act as a size-selective filter, allowing smaller particles to pass while excluding larger ones [20, 21]. However, such structural filtration mechanisms are inherently static, offering limited tunability once fabricated [22] and often leading to a trade-off between selectivity and permeability [23]. Alternatively, chemical selectivity has been introduced through dynamic bonding interactions, such as reversible ligand binding [24, 25], host–guest chemistry [26], or charge-based interactions [27], which can selectively impede or promote transport of specific species. While effective in certain cases, these approaches typically require complex chemical functionalization, may suffer from limited reversibility and reusability, and are often sensitive to environmental conditions such as pH, ionic strength, or solvent composition [25]. Consequently, there remains a strong need for a physically programmable, dynamically tunable approach to selective particle diffusion that does not rely solely on static structure or permanent chemistry.

Recently, mechano-diffusion has emerged as a promising physical route for modulating transport in hydrogel media [28, 29]. By applying static or quasi-static mechanical deformation, such as stretching or torsion, the polymer network structure and stored elastic energy can be tuned, thereby altering the energy barriers that particles must overcome to hop between adjacent mesh cavities [30, 31]. This mechanical tuning enables controllable enhancement of diffusivity and provides a means to promote transport along preferred directions. However, existing mechano-diffusion strategies are largely limited to static or slowly varying loading conditions, so that under quasi-static deformation, all particles experience similar shifts in the energy landscape, making it challenging to generate strong, time-dependent selectivity between particles.

Herein, to overcome these limitations, we introduce ultrasound as a dynamic, high-frequency mechanical stimulation to actively program selective diffusion in hydrogel systems. Ultrasonic excitation simultaneously interacts with both the particles and the polymer network, but its effects are intrinsically size-dependent [32, 33]. For particles smaller than the mesh size, the acoustic field induces localized thermal and vibrational energy fluctuations, effectively increasing the particle hopping energy and enhancing their mobility [34, 35]. In contrast, for particles larger than the mesh size, transport is governed by polymer network deformation, where ultrasound induces transient rearrangement, oscillation, and local expansion of polymer meshes [34, 36], leading to time-dependent modulation of the energy barrier. Because smaller particles can more efficiently absorb and respond to the high-frequency thermal and mechanical energy [37], their diffusivity is enhanced more significantly than that of larger particles, resulting in an amplified diffusivity contrast between particles under ultrasonic stimulation. To investigate and demonstrate particle diffusion selectivity, we developed an Ultrasound Diffusion Characterization Platform (UDCP), to observe the model particle-hydrogel system diffusion under ultrasonic stimulation, which consists of polyacrylamide (PAAm) hydrogels loaded with fluorescent particles spanning a wide range of hydrodynamic sizes, including FITC–dextran and Rhodamine B (RhB). For the individual FITC–dextran particles, the low- and intermediate-power ultrasonic stimulations can enhance the diffusion across all sizes, while the high-power ultrasound can induce a non-monotonic trend of diffusion profile due to polymer network damage. For dual FITC–dextran and Rhodamine B particles, ultrasonic stimulation can demonstrate strong particle diffusion selectivity under moderate power levels. The presented framework establishes ultrasound as a powerful tool for selective diffusion engineering, with broad implications for targeted drug delivery, smart filtration systems, environmental sensing, and adaptive soft material platforms. It should be noted that although this work examines the effect of ultrasound power on molecular release and transport behavior, the ultrasonic setup used here does not directly correspond to the operating conditions of current medical ultrasound devices. Accordingly, the purpose of this study is not to directly replicate a clinical ultrasound configuration, but rather to establish and validate the underlying concept that ultrasound can function as a programmable dynamic mechanical stimulus for regulating the relative transport of different molecules in hydrogel networks and thereby enabling selective release.

Ultrasound-Diffusion Characterization Platform

To systematically investigate mechano-acoustic modulation of particle transport in deformable polymer networks, we first build an ultrasound diffusion characterization platform (UDCP). UDCP integrates a controllable ultrasonic excitation system with a miniaturized uniaxial stretching device within a single diffusion setup, enabling orthogonal regulation of the hydrogel structural state and externally injected acoustic energy. By imposing a prescribed stretch ratio on a hydrogel while introducing separately tunable ultrasound

stimulation, this platform establishes a dual-variable control environment. This design allows both decoupled and coupled evaluation of mechanical deformation and acoustic energy contributions to particle diffusion behavior (Fig. 1A).

Within the UDCP, hydrogels are mounted onto a custom miniaturized stretcher, where the stretch ratio can be continuously adjusted and stably maintained to define the polymer network configuration. Simultaneously, a probe-type sonicator immersed in the surrounding solution bath provides independently controllable acoustic energy input, with acoustic power, duty cycle, and exposure duration prescribed as tunable parameters (Fig. 1B). The external bath, whose volume is significantly larger than that of the hydrogel, functions as an effective infinite sink, establishing a stable concentration gradient that drives outward diffusion while preventing boundary concentration accumulation from influencing transport behavior. Under these strictly controlled structural and boundary conditions, ultrasound acts as an independent energy field that modulates the kinetics of particle transport across the polymer network energy barrier. By comparing passive diffusion in the absence of ultrasound with energy-assisted transport under identical mechanical constraints, UDCP enables quantitative decoupling of structural effects from acoustic energy contributions to transport behavior.

To demonstrate the feasibility and stability of UDCP, PAAm hydrogels and FITC–dextran are employed as a representative model system. PAAm provides a mechanically predictable polymer network with large deformability (Fig. 1C), while FITC–dextran serves as a well-characterized fluorescent particle for quantitative release analysis. It is worth noting that this PAAm–FITC system is used as a proof-of-concept validation to demonstrate the functional capability of the platform, rather than to establish material-specific conclusions. The underlying design principles and control logic of UDCP can be extended to diverse hydrogel chemistries and diffusing species of varying sizes and physicochemical properties, thereby providing a general experimental framework for constructing mechano-acoustic transport maps in deformable soft materials.

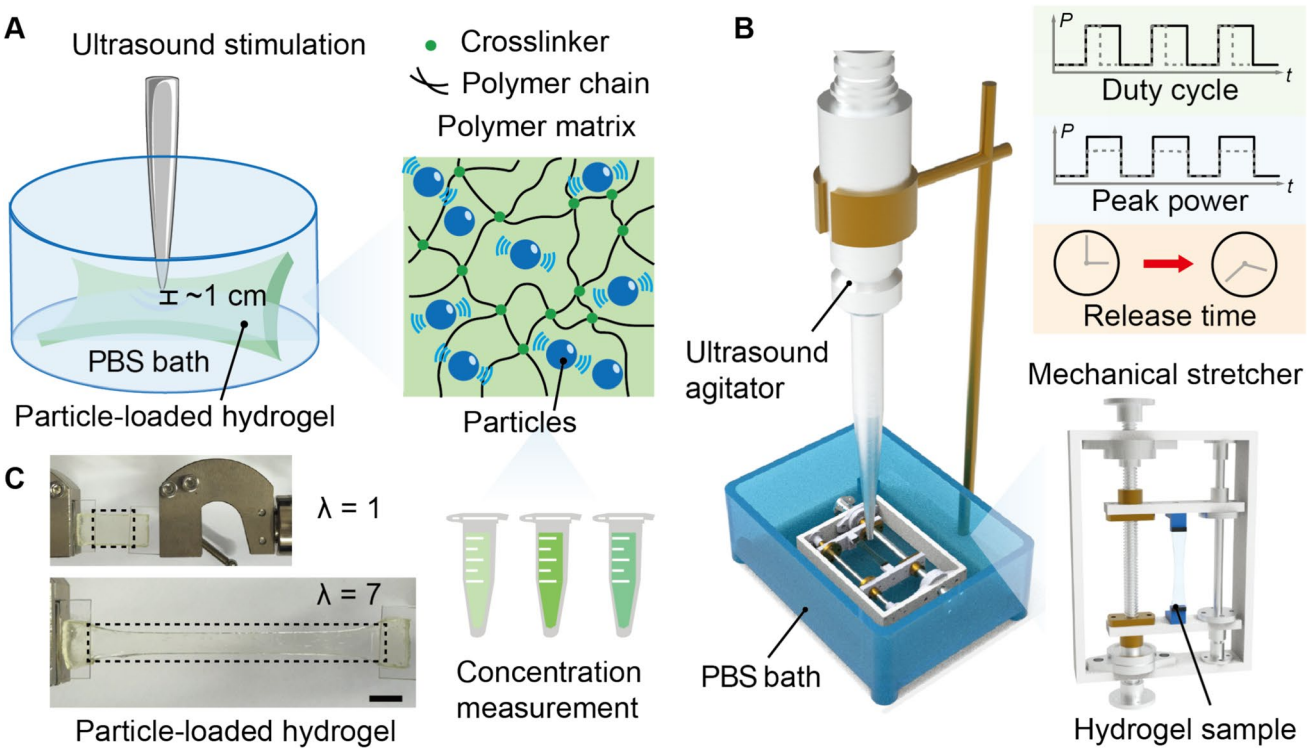


Fig. 1 Ultrasound Diffusion Characterization Platform (UDCP) for ultrasound-mediated particle release from hydrogels. (**A**) Schematic of a particle-loaded hydrogel immersed in a phosphate-buffered saline (PBS) bath under ultrasonic stimulation. The inset shows a crosslinked polymer network with embedded particles undergoing acoustically assisted transport. **(B)** Schematic of the ultrasound diffusion characterization platform. (Left) An ultrasound probe delivers pulsed acoustic stimulation to a hydrogel sample immersed in a PBS bath, with controlled duty cycle, peak power, and release time. (Right) A miniaturized mechanical stretcher enables in situ hydrogel deformation for release characterization. **(C)** Optical images of a particle-loaded hydrogel sample at stretch ratios of $\lambda = 1$ and $\lambda = 7$. Scale bar: 2 cm.

Working Principle

In ultrasound-modulated particle release from hydrogels, the underlying transport behavior is governed by distinct fundamental mechanisms that depend on the size relationship between the diffusing particle (d) and the network mesh (ξ). When the particle size is smaller than the mesh size, transport primarily follows a continuous Brownian diffusion regime. In this regime, the diffusion rate is predominantly determined by particle kinetic energy and local viscous resistance [38]. Under ultrasonic stimulation, periodic acoustic energy input enhances particle velocity fluctuations and vibrational amplitudes, effectively increasing the particle's kinetic activity and accelerating release. Such particles are not geometrically confined by the polymer network; ultrasound-driven acceleration arises mainly from enhanced particle dynamics (Fig. 2A, upper right). When the particle size becomes comparable to or larger than the mesh size, the transport mechanism changes fundamentally. Larger particles are transiently confined within cage-like structures formed by the surrounding polymer chains, and their motion is no longer governed solely by continuous Brownian motion (Fig. 2A, lower right). Instead, particle transport proceeds through an obstruction- or hopping-dominated process, in which the particle must overcome an energy barrier associated with network elasticity, local chain constraints, and particle–network interactions. Therefore, for large particles, the release rate depends not only on particle mobility in the solvent phase, but also on the probability of successful barrier-crossing events.

Ultrasound modulates these two transport regimes through coupled kinetic and structural effects (Fig. 2B). For small particles, ultrasound primarily enhances particle velocity fluctuations and vibrational motion within the hydrogel pores, thereby increasing the effective kinetic activity of the diffusing species and accelerating Brownian diffusion. Because these particles are not strongly constrained by the polymer network, the ultrasound-induced enhancement mainly arises from increased particle motion rather than from substantial changes in network confinement [39]. For larger particles, ultrasound has a more complex effect. In addition to increasing particle vibrational activity and the frequency of attempts to cross local barriers, ultrasound also excites dynamic fluctuations of the polymer chains surrounding the particle. These chain fluctuations induce transient rearrangements of the local cage structure and cause temporal variations in the effective energy barrier. As a result, the barrier height is not fixed, but fluctuates around a mean level under ultrasonic excitation. Moments of reduced barrier height increase the probability of successful hopping events, thereby promoting the release of large particles that would otherwise be more strongly confined by the network. In addition to these internal transport effects, acoustic streaming may also contribute to the observed ultrasound-enhanced release behavior.

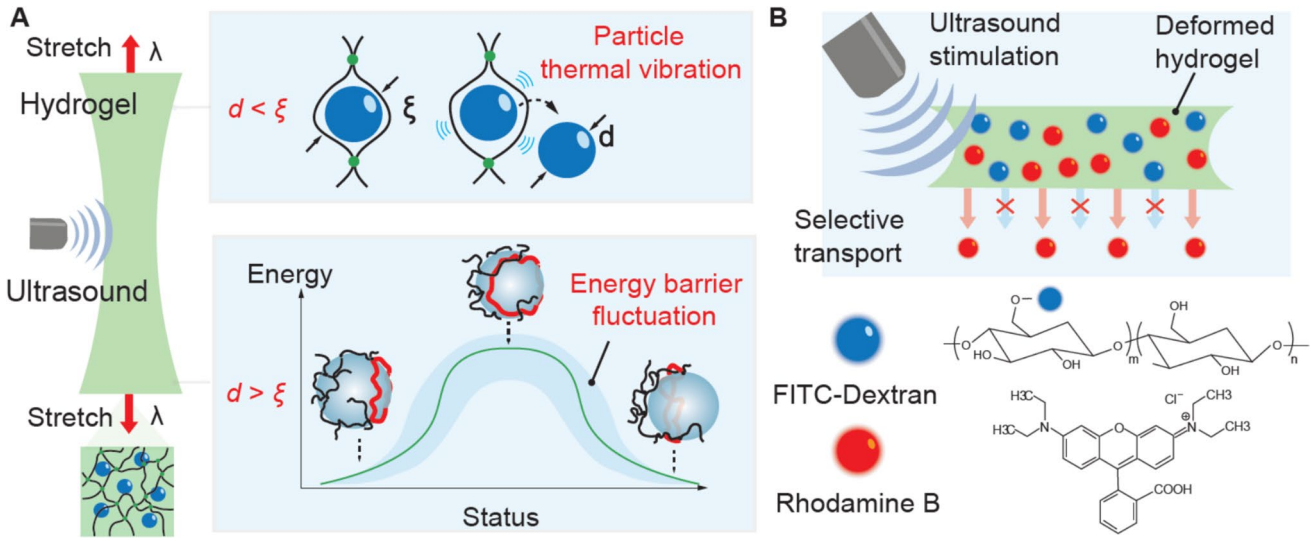


Fig. 2 Mechanism of ultrasound-mediated selective particle transport in stretched hydrogels. (**A**) Schematic of mechano-diffusion of particles in a stretched polymer network, highlighting the role of the ratio between particle diameter (d) and network mesh size (ξ). When $d<\xi$, particle motion is dominated by thermally driven Brownian vibration within the polymer network; when $d>\xi$, particle transport requires overcoming an energy barrier associated with network deformation. Ultrasound introduces additional mechanical fluctuations that dynamically modulate the energy barrier and enhance particle hopping. (**B**) Illustration of ultrasound-amplified selective transport in a deformed hydrogel. Under acoustic stimulation, smaller particles (e.g., Rhodamine B) preferentially migrate through the network, whereas larger particles (e.g., FITC–dextran) remain confined, resulting in size-dependent selective release.

Mechanical stretching provides a structurally distinct mode of transport regulation. Unlike ultrasound, which acts as a dynamic mechanical energy input, stretching primarily changes the geometric configuration of the polymer network. By deforming the hydrogel, stretching alters mesh size, transport pathways, local chain orientation, and the baseline energy landscape encountered by diffusing particles. Therefore, stretching mainly regulates the mean confinement condition and mean barrier level, whereas ultrasound mainly enhances the temporal fluctuation amplitude of particle motion and network constraints. Depending on the particle size and network structure, stretching and ultrasound may act synergistically or competitively in regulating particle release.

In the present system, Rhodamine B serves as a representative small-molecule tracer whose molecular size is smaller than the average mesh size of the hydrogel network. Its release is therefore mainly governed by Brownian diffusion and is accelerated under ultrasound primarily through enhanced molecular motion. In contrast, FITC–dextran with multiple molecular weight represents a larger macromolecular tracer with hydrodynamic sizes comparable to or exceeding the network mesh size. Its release is governed by both solvent-phase mobility and network-mediated confinement, making it more sensitive to ultrasound-induced fluctuations of the polymer network and the associated energy barrier. Because Rhodamine B and FITC–dextran operate under different transport regimes, they do not respond proportionally to the same external stimulus. A global ultrasound input can accelerate the release of both species, but the underlying enhancement pathways are different. Rhodamine B mainly responds through increased Brownian mobility, whereas FITC–dextran responds through a combination of enhanced particle motion, increased hopping attempt frequency, and dynamic reduction of network confinement barriers. This difference in stimulus sensitivity reshapes the relative release rates of the two species and can amplify selective release. In this context, selectivity does not arise from ultrasound targeting one specific molecule directly, but from the intrinsic mismatch between particle size, network constraints, and the way external mechanical energy couples to each transport mechanism.

Theoretical Analysis

The above mechanism can be further interpreted using a minimal theoretical framework for ultrasound-assisted dynamic transport (Fig. 3). Ultrasound does not introduce a separate transport law; rather, it renders the key variables in the obstruction and hopping models explicitly time dependent. Under ultrasonic excitation, the effective mesh size can be expressed as $\xi(t)$, reflecting transient changes in local network confinement. The strain energy stored in the surrounding polymer chains becomes $W(t)$, which further modulates the hopping energy barrier $\Delta U(t)$. At the same time, enhanced particle vibration within the solvent phase may increase the intrinsic liquid-phase diffusivity, D_{liq}, and the corresponding frequency of barrier-crossing attempts. Together, these time-dependent variables regulate the instantaneous confinement condition, hopping probability, and macroscopic release kinetics under mechano-acoustic stimulation.

Accordingly, the instantaneous diffusivity under ultrasound can be expressed in the generic form

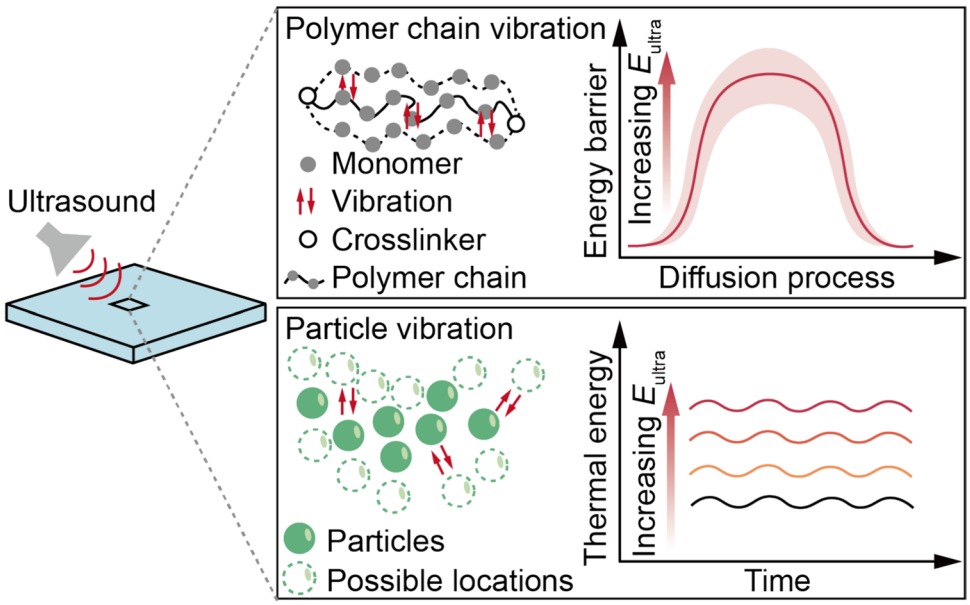


Fig. 3 Conceptual framework of ultrasound-induced mechano-diffusion in polymer networks. Ultrasound acts as a dynamic mechanical perturbation that simultaneously modulates the deformation state of surrounding polymer chains and the kinetic activity of embedded particles. These coupled effects induce temporal fluctuations in the local hopping barrier and particle kinetic energy, thereby modulating the probability of cage escape and giving rise to time-dependent particle diffusivity within polymer networks.

$$D(t) = D_{obs}\left(\frac{d}{\xi(t)}\right)\exp\left[-\frac{\Delta U(W(t), d/\xi(t))}{k_B T}\right] \quad (1)$$

where D_{obs} refers to obstruction diffusivity. The experimentally relevant diffusivity is the cycle-averaged quantity

$$D_{\text{eff}} = \langle D(t)\rangle_t \quad (2)$$

This formulation indicates that diffusion enhancement under ultrasound arises from nonlinear time averaging of oscillatory modulation of steric confinement and activation barrier, rather than from a purely static structural change.

The role of ultrasound parameters can also be understood within this framework. The ultrasonic power (or intensity), denoted by P, primarily determines the amplitude of the acoustic pressure and thus the magnitude of the induced oscillatory strain ε_a, whereas the ultrasound frequency, denoted by f, sets the timescale of oscillation. In this sense, the oscillatory strain amplitude may be written as

$$\varepsilon_a = \varepsilon_a(P,f) \quad (3)$$

where P and f denote the applied ultrasonic power and frequency, respectively. The effective diffusivity may therefore be expressed as

$$D_{\text{eff}} = D_{\text{eff}}(P,f,d,\xi_0) \quad (4)$$

where d is the particle diameter and ξ_0 is the undeformed mesh size. In the small-amplitude regime, the leading-order enhancement in the cycle-averaged diffusivity scales quadratically with the oscillatory strain amplitude,

$$\Delta D_{\text{eff}} \propto \varepsilon_a^2 \quad (5)$$

so that D_{eff} generally increases with increasing ultrasonic power. By contrast, the role of frequency is more intricate because it controls whether the polymer network and solvent can fully respond within each oscillation cycle, and it may also affect the onset and intensity of acoustic cavitation and mechanical coupling effects. The present framework is intended as a minimal physical description linking dynamic stress, effective mesh size, and diffusivity, rather than as a full acoustic-poroelastic model.

Materials and Methods

Synthesis of Particle-Loaded Hydrogels

Unless otherwise specified, all chemicals were purchased from Sigma-Aldrich and used as received. To prepare the hydrogel precursor, 0.75 g acrylamide (AAm) was dissolved in 2.5 mL phosphate-buffered saline (PBS). Subsequently, 0.25 mL of 0.23 wt.% N,N′-methylenebis(acrylamide) (MBAA) was added as the crosslinker, followed by 50 µL of 10 wt.% ammonium persulfate (APS) as the thermal initiator and 2.5 µL of N,N,N′,N′-tetramethylethylenediamine (TEMED) as the accelerator. This formulation corresponded to an estimated average mesh size of approximately 15.96 nm [40].

For ultrasound-mediated mechano-diffusion experiments, 2.5 mg of FITC–dextran with molecular weights of 4, 70, 150, or 250 kDa was separately added to the precursor solution. The corresponding estimated hydrodynamic diameters were approximately 2.6, 10.8, 15.8, and 20.4 nm respectively [41], giving particle-to-mesh size ratios (d/ξ, with $\xi \approx 15.96$ nm) of approximately 0.16, 0.68, 1.0, and 1.3. For ultrasound-mediated selective release experiments, 30 mg FITC–dextran and 360 µL Rhodamine B solution (1 mg/mL) were added to the precursor. The concentration was selected according to the sensitivity range of the measurement instrument to ensure that the concentration change within the first hour remained detectable.

The precursor solutions were mixed and defoamed using a centrifugal mixer (AR-100, THINKY), purged with nitrogen gas to remove residual oxygen, and cast into acrylic molds (20 mm × 10 mm × 3 mm) to obtain hydrogel samples of identical dimensions. The molds were fabricated by laser cutting (Epilog Laser) and consisted of a hollow acrylic chamber and a top cover plate. Polymerization was carried out on a hotplate at 60 °C for 30 min. During curing, the precursor solution was covered with a glass slide, and the mold was tightly clipped to maintain sealing, thereby minimizing oxygen exposure and suppressing inhibition of free-radical polymerization. The molds were additionally wrapped in aluminum foil to minimize dye exposure to light during curing. After polymerization, the hydrogels were removed from the molds for subsequent experiments.

The theoretical maximum release concentration of FITC–dextran or Rhodamine B in the surrounding medium was calculated assuming complete equilibibration of all molecules initially contained within the hydrogel with the external medium.

Ultrasound-mediated Release Experiments

Ultrasonic stimulation was applied using a Branson 450 Sonifier probe-type ultrasonic processor (VWR Scientific). The device operated at approximately 20 kHz, with output power and duty cycle controlled during the experiments. According to the manufacturer's manual, the horn frequency range is 19.850–20.050 kHz, and the Model 450 has a maximum output power of 400 W. A particle-loaded hydrogel specimen was placed in an opaque paper cup and immersed in phosphate-buffered saline (PBS). For ultrasound-modulated release enhancement experiments, 20 mL of PBS was used as the bath volume, whereas 10 mL was used in

ultrasound-mediated selectivity experiments due to differences in concentration measurement requirements. The probe was fixed directly above the center of the hydrogel sample at an approximate distance of 1 cm (Fig. 1A), with the probe tip immersed in the surrounding water medium. The container was covered with aluminum foil during stimulation to minimize light exposure. At 10 min intervals, aliquots of the bath solution were withdrawn for concentration measurement.

Mechanical Characterizations of Bulk Hydrogel

All mechanical tests were performed using a U-Stretch testing device (CellScale). Bulk hydrogel samples were trimmed to dimensions of 5 cm × 2 cm. Both ends of each hydrogel film were sandwiched between two acrylic plates (5 cm × 2 cm), and additional acrylic holders (1 cm × 0.5 cm) were attached at the ends, leaving a 1 cm gauge length for stretching. The assembled sample was then immersed in a PBS bath and exposed to ultrasound at controlled intensities. For the stress relaxation test, the hydrogel was stretched to a stretch ratio of $\lambda = 3$, and the subsequent stress evolution was recorded over time. For the pure-shear tensile test, the hydrated hydrogel thickness was first measured, after which the sample was mounted vertically on the U-Stretch testing device and stretched at a rate of 1 mm/s until failure. For notched samples, the same procedure was followed except that a approximately 1-cm notch was introduced at the center of the hydrogel prior to testing. Fracture toughness was determined from the experimental results of both notched and unnotched samples, while Young's modulus was calculated from the initial slope of the stress–stretch curve obtained from the unnotched samples.

Concentration Measurement in PBS Bath

For release enhancement experiments involving single-component FITC–dextran, particle concentration in the PBS bath was quantified using a Qubit 4 Fluorometer (ThermoFisher Scientific). Prior to measurement, blank PBS was used for baseline calibration. At each time, approximately 200 µL of the bath solution was withdrawn for fluorescence analysis. After measurement, the sampled solution was returned to the bath to maintain a constant total volume throughout the experiment. For selective diffusion experiments involving both FITC–dextran and Rhodamine B, concentration analysis was performed using a NanoDrop microvolume UV–Vis spectrophotometer (ThermoFisher Scientific). UV–Vis spectroscopy was employed to capture the full absorption spectrum, enabling spectral discrimination between FITC–dextran and Rhodamine B based on their characteristic absorbance peaks (~490 nm for FITC–dextran and ~550 nm for Rhodamine B). Calibration curves were established using solutions of known concentrations prior to release measurements. At each sampling interval, 5–10 µL of the bath solution was collected for analysis. Due to the negligible sampling volume relative to the total bath volume, the aliquots were not returned to the system.

Calculation of Diffusivity, Normalized Diffusivity, and Selectivity

To quantitatively compare transport capability under different conditions, the apparent effective diffusivity was calculated based on the early-stage change in normalized concentration [42, 43]. First, the measured bath concentration in the release profile was normalized as $C_{norm}(t)$, defined as the concentration at time t divided by the estimated maximum bath concentration assuming complete release of all loaded molecules into the bath. In the early diffusion-controlled stage, the change in normalized concentration can be approximated as [42]:

$$C_{norm}(t) = 4\left(\frac{Dt}{\pi h^2}\right)^{1/2} \tag{6}$$

where D is the diffusivity and h is the effective diffusion length. Since the hydrogel can release solutes from both sides, h was approximated as half of the total hydrogel thickness to represent the effective diffusion distance along one release direction.

According to the above relationship, the normalized concentration is approximately linear with $\sqrt{t}$:

$$C_{norm}(t) \propto \frac{\sqrt{D}}{h}\sqrt{t} \tag{7}$$

Therefore, the early-stage normalized concentration profile was fitted as:

$$C_{norm}(t) = k\sqrt{t} + b \tag{8}$$

where k is the fitted slope of $C_{norm}(t)$ versus $\sqrt{t}$, and b is the intercept ($b = 0$ at all times). Based on the square-root-of-time relationship between $C_{norm}(t)$ and D, the fitted slope k satisfies:

$$k \propto \frac{\sqrt{D}}{h} \tag{9}$$

Thus, the apparent effective diffusivity was estimated from the slope of the normalized concentration profile with respect to $\sqrt{t}$:

$$D_{eff} = (kh)^2 \tag{10}$$

To further compare relative transport capability under different conditions, the apparent effective diffusivity was normalized by that under the corresponding control condition. The normalized diffusivity was defined as:

$$D_{norm} = \frac{D_{eff,i}}{D_{eff,0}} \tag{11}$$

where $D_{eff,i}$ is the apparent effective diffusivity under condition i (under ultrasound stimulation, mechanical stretching, or their combined application), and $D_{eff,0}$ is that under the corresponding control condition. Because all samples used the same hydrogel thickness and the same definition of the effective diffusion layer thickness h, the h term cancels during normalization:

$$D_{norm} = \left(\frac{k_i}{k_0}\right)^2 \tag{12}$$

where k_i and k_0 are the fitted slopes obtained from the early-stage normalized concentration profiles under condition i and the control condition, respectively. Therefore, although the estimation of D_{eff} includes the effective diffusion layer thickness h, h does not affect the final relative comparison when calculating D_{norm}. In other words, D_{norm} reflects the relative change in the squared slope of the early-stage normalized concentration profile.

Selectivity, S, was defined as the ratio of the apparent effective diffusivities of two different molecules under the same condition. For example, for Rhodamine B (RhB) and FITC–dextran, selectivity was calculated as:

$$S = \frac{D_{eff,RhB}}{D_{eff,FITC-dextran}} = \left(\frac{k_{RhB}}{k_{FITC-dextran}}\right)^2 \tag{13}$$

This parameter was used to quantify the relative transport preference of the hydrogel for one molecule over another.

Results

Effect of Ultrasound on FITC–Dextran Release

The effect of ultrasound stimulation on FITC–dextran transport was quantitatively evaluated using the calibration relationships established for tracers of different molecular weights (4, 70, 150, and 250 kDa) in Fig. 4. The strong linear relationship between fluorescence intensity and concentration enabled reliable conversion of fluorescence

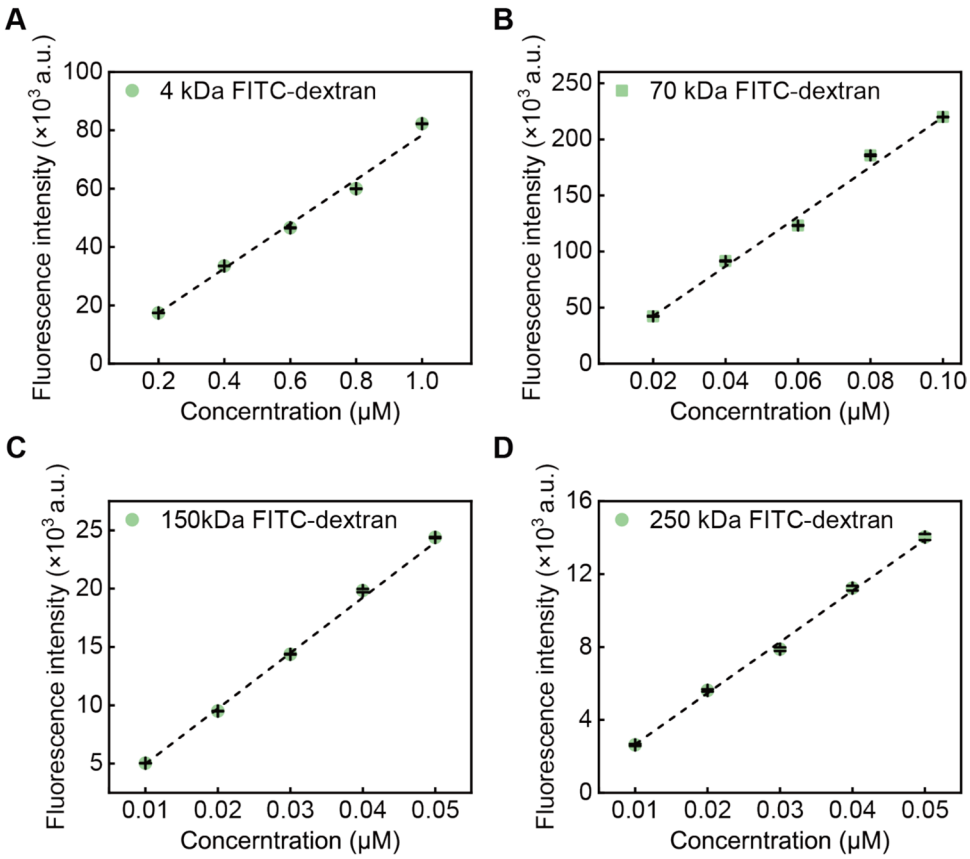


Fig. 4 Fluorescence intensity calibration curves for FITC-dextran molecules with different molecular weights. Linear relationships between fluorescence intensity and concentration are shown for **(A)** 4 kDa, **(B)** 70 kDa, **(C)** 150 kDa, and (**D**) 250 kDa FITC–dextran. Dashed lines represent linear regression fits used for concentration quantification. Values represent mean ± SD ($n = 5$).

signals into FITC–dextran concentrations in the PBS bath. Based on these calibrations, time-dependent release profiles from stretched hydrogels were obtained under both ultrasound and control (no ultrasound) conditions. For all molecular weights, the FITC–dextran concentration in the surrounding PBS bath increased monotonically with time, indicating continuous outward diffusion driven by concentration gradients.

Ultrasound enhanced the release of all FITC–dextran species, although the magnitude of this enhancement depended strongly on molecular size. As shown in Fig. 5A–D, the release profiles obtained under ultrasound were consistently higher than those measured without ultrasound for 4, 70, 150, and 250 kDa FITC–dextran. Because all samples were prepared using the same mass of FITC–dextran, their initial molar concentrations differed by molecular weight. To enable direct comparison across molecular sizes, the release data were therefore normalized by the estimated maximum concentration, $C_{\max}$, defined as the concentration that would be reached assuming the complete equilibration of FITC–dextran initially loaded in the hydrogel with the PBS bath. After normalization, the early-stage release behavior became directly comparable: within the first hour, the normalized concentration for all four FITC–dextran species was approximately 0.1 in the absence of ultrasound and increased to about 0.2–0.3 under ultrasonic stimulation (Fig. 5E–H). This result shows that under the same stretching and ultrasound conditions, ultrasound affects the release of different FITC–dextran species to different extents.

To further compare transport behavior across molecular weights, the corresponding molar concentrations associated with complete release were calculated, as summarized in Fig. 6A. Because the same mass of FITC–dextran was used in all cases, the molar concentration decreased with increasing molecular weight. In particular, 4 kDa FITC–dextran exhibited a substantially higher molar concentration, approximately 6.5 μM, whereas the concentrations of the 70, 150, and 250 kDa species were much lower, ranging from about 0.1 to 0.37 μM. Effective diffusivities were then extracted by fitting the early-stage release profiles.

However, the relative increase in diffusivity was distinctly non-monotonic with molecular weight (Fig. 6B). The largest enhancement was observed for 150 kDa FITC–dextran, followed by 70 kDa, whereas the increase was comparatively modest for both the smallest (4 kDa) and largest (250 kDa) species. This behavior indicates that the effect of ultrasound cannot be interpreted as a simple monotonic function of molecular size, but instead reflects distinct transport regimes associated with particle size relative to the hydrogel mesh. For 4 kDa FITC–dextran, transport is only weakly hindered by the network under baseline conditions, so ultrasound provides limited additional enhancement. In contrast, 250 kDa FITC–dextran is much more strongly confined within the network, and ultrasound is insufficient to shift a substantial fraction of molecules from a trapped state into an effectively releasable regime. By comparison, the intermediate-sized 70 and 150 kDa species fall within a transport regime that is especially sensitive to ultrasound-induced perturbations of polymer chain dynamics and transient transport pathways,

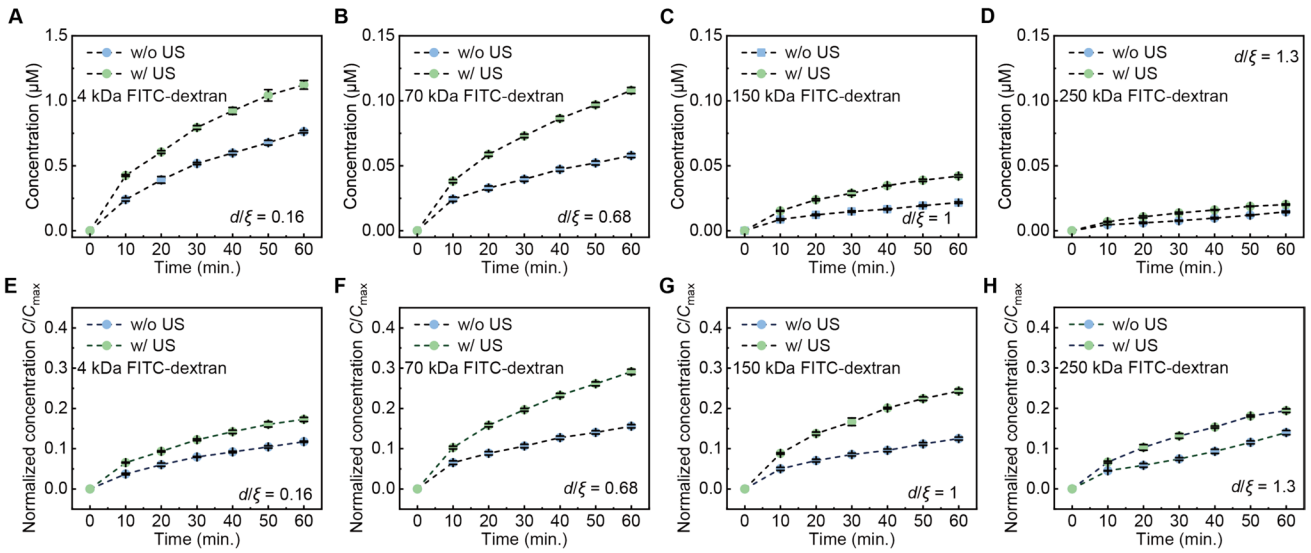


Fig. 5 Ultrasound-mediated release kinetics of FITC–dextran with different molecule weights. Time-dependent release concentration profiles of (**A**) 4 kDa, (**B**) 70 kDa, (**C**) 150 kDa, and (**D**) 250 kDa FITC–dextran from stretched hydrogels under conditions with and without ultrasound stimulation. Corresponding normalized release profiles (C/C_{max}) are shown in (**E–H**). All hydrogels were tested under a stretching ratio of $\lambda = 2$ and an ultrasound output power of 4. Data are presented as mean ± SD ($n = 3$).

A

Molecular weight (kDa)	Mass concentration (mg/mL)	Molar concentration (μM)
4	0.0260	6.4956
70	0.0260	0.3712
150	0.0260	0.1731
250	0.0260	0.1039

B

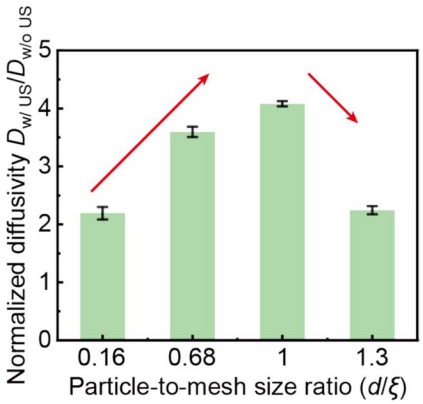


Fig. 6 Concentration normalization and diffusivity comparison of FITC–dextran with different molecular weights. (**A**) Calculated mass and molar concentrations of the four FITC–dextran species in the PBS bath, assuming complete release from the hydrogel. (**B**) Ultrasound-mediated diffusivity, quantified by the normalized diffusivity ratio ($D_{w/US}/D_{w/oUS}$), as a function of the particle-to-mesh size ratio (d/ξ). Data in (**B**) are presented as mean ± SD ($n = 3$).

resulting in the greatest relative increases in diffusivity and release.

This non-monotonic size dependence is consistent with the dual-mechanism framework described in the above section. In the small-particle regime relative to the mesh size, ultrasound mainly enhances transport by increasing particle kinetic activity through mechanical vibration and thermal agitation. In the large-particle regime, ultrasound can additionally promote transient network deformation and rearrangement, thereby lowering the effective transport barrier. The strongest enhancement therefore occurs in an intermediate size range, where ultrasound is sufficient to activate barrier-limited transport, but the particles are not yet so strongly confined that release remains largely suppressed.

It should also be noted that the local acoustic pressure experienced by the hydrogel depends on the probe–sample distance and relative positioning. In addition, due to the geometry of the transducer, the acoustic field is expected to be spatially non-uniform, which may generate heterogeneous streaming patterns and non-uniform enhancement of local mass transport. Although the probe position and sample placement were kept constant across experiments to improve reproducibility, such field heterogeneity may still contribute to experimental variability and should be considered when interpreting ultrasound-regulated diffusion behavior. Overall, these results demonstrate that the effect of ultrasound on nanoparticle transport is highly dependent on particle size and transport regime. Rather than producing a uniform enhancement across all species, ultrasound most effectively promotes the release of intermediate-sized molecules, for which transport is particularly sensitive to perturbations in polymer chain dynamics and transient transport pathways.

Comparison between Strain Effect and Ultrasound Stimulation

According to our previous studies, static or quasi-static mechanical deformation of polymer networks can increase nanoparticle diffusivity by altering mesh size and network elasticity [28]. After establishing that ultrasound increased the release and diffusivity of all FITC–dextran species, we selected 150 kDa FITC–dextran, corresponding to $d/\xi \approx 1$, as a representative system for further comparison of the individual and combined effects of mechanical stretching and ultrasound. This molecular size exhibited the largest diffusivity enhancement under ultrasound and therefore represents the transport regime most sensitive to external perturbation. To directly compare the effectiveness of these two stimuli, a series of controlled experiments was performed using hydrogels loaded with 150 kDa FITC–dextran. In the first set of experiments, no ultrasound was applied, and the hydrogels were subjected to different uniaxial stretch ratios of $\lambda = 1.0$, 1.5, and 2.0 (Fig. 7A). In the second set, the hydrogels were maintained in the undeformed state ($\lambda = 1.0$) and exposed to ultrasound at two power levels, namely low power and intermediate power (Fig. 7C). The corresponding normalized diffusivity values are summarized in Fig. 7B and D.

Under purely mechanical stretching conditions without ultrasound, the release concentration increased with increasing stretch ratio, confirming that static deformation facilitates transport by enlarging the effective mesh size and reducing diffusion resistance along the loading direction. Among the three stretch conditions, the hydrogel at $\lambda = 2.0$ consistently showed the highest release, followed by $\lambda = 1.5$ and $\lambda = 1.0$. However, the overall enhancement in diffusivity remained moderate, reaching only about 1.5-fold even at $\lambda = 2.0$. In contrast, under ultrasound stimulation in the absence of stretch, a more pronounced increase in both release and diffusivity was observed. At intermediate ultrasound power, the diffusivity increased by approximately 1.75-fold relative to the no-ultrasound condition. Direct comparison further showed that hydrogels exposed to intermediate-power ultrasound without stretching exhibited higher release concentrations than hydrogels subjected to mechanical stretching alone, even at the largest stretch ratio tested ($\lambda = 2.0$). These results indicate that for the 150 kDa

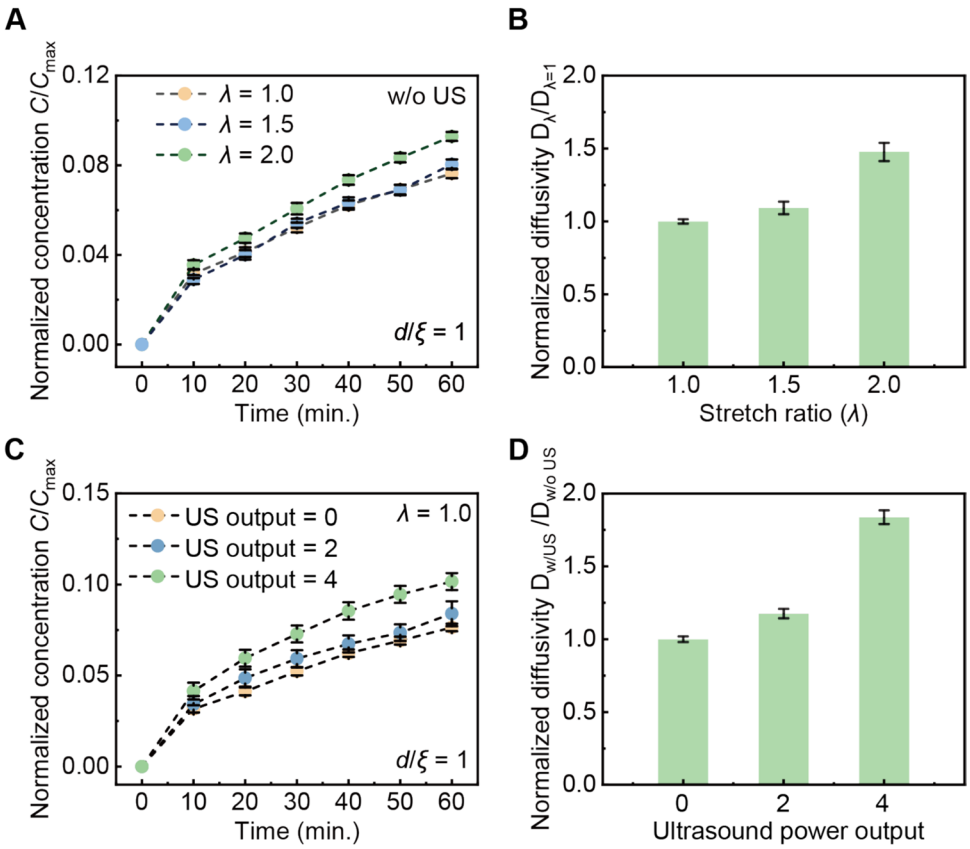


Fig. 7 Effects of mechanical stretch and ultrasound power. (**A**) Time-dependent normalized release profiles (C/C_{max}) of 150 kDa FITC-dextran from hydrogels under different stretch ratios ($\lambda = 1.0, 1.5, 2.0$) without ultrasound stimulation, and **(B)** the corresponding normalized diffusivity ($D_\lambda/D_{\lambda=1}$). **(C)** Time-dependent release profiles of 150 kDa FITC-dextran at $\lambda = 1.0$ under low and intermediate ultrasound powers, and **(D)** the corresponding normalized diffusivity ($D_{w/US}/D_{w/oUS}$). The particle-to-mesh size was maintained at $d/\xi = 1$. Values represent mean ± SD ($n = 3$).

tracer, dynamic acoustic stimulation is more effective than static mechanical deformation in promoting transport.

Although both stretching alone and ultrasound alone enhanced transport, the increase became substantially greater when the two perturbations were applied simultaneously. Under the combined action of stretching and ultrasound, the normalized diffusivity increased by nearly fourfold (Fig. 6B), far exceeding the enhancement produced by either stimulus alone. This result indicates a synergistic interaction between stretching and ultrasound for particles in this size regime. Rather than simply contributing independent effects, the two perturbations appear to cooperatively lower the effective transport barrier and promote escape from transient confinement within the polymer network.

This synergistic behavior is consistent with the particle-to-mesh-size-dependent mechano-diffusion framework. For particles much smaller than the mesh size, ultrasound mainly enhances transport by increasing particle and matrix fluctuations, whereas stretching contributes only a modest additional effect through geometric modification of the network. For particles much larger than the mesh size, both perturbations remain insufficient to shift transport substantially away from a strongly trapped state. The strongest response is expected when particle size is comparable to, or slightly larger than, the mesh size, where transport is dominated by hopping across transient polymer cages. In this regime, ultrasound-induced fluctuations and stretch-induced geometric opening can act together to facilitate cage escape, leading to a much stronger enhancement of diffusivity and release than either perturbation alone.

High Power Ultrasonic Stimulation Effect

Under high-power ultrasonic stimulation, the release behavior of FITC–dextran exhibited a qualitatively different profile from that observed under low-power conditions. As shown in Fig. 8A, the normalized FITC–dextran concentration no longer increased monotonically with time, but instead displayed a transient decrease after the initial rapid release stage. This behavior contrasts sharply with the steadily increasing release profile obtained under low-power ultrasound, indicating that high-power ultrasound does not simply produce a stronger version of diffusion enhancement, but instead changes the governing transport process.

To exclude the possibility that this anomalous release profile arose from an optical measurement artifact, we continuously monitored the fluorescence intensity of pure FITC–dextran and Rhodamine B solutions under the same ultrasound conditions in the absence of hydrogel. In both cases, no noticeable decrease in fluorescence intensity was observed over 1 h of sonication. These control experiments indicate that the transient concentration decrease observed in Fig. 8A is unlikely to

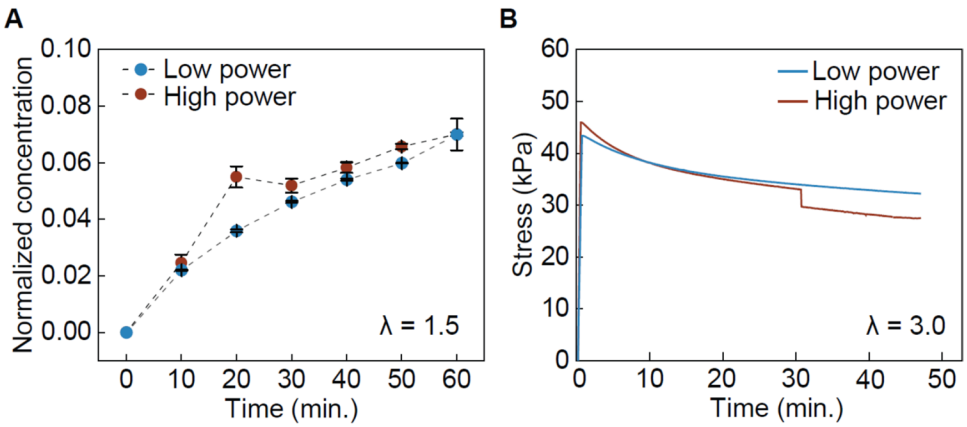


Fig. 8 Effects of high-power ultrasound on particle release and hydrogel degradation. **(A)** Time-dependent normalized concentration of released particles from stretched hydrogels (λ = 1.5) under low- (Output = 4) and high-power (Output = 8) ultrasound stimulation. High power initially enhances release but exhibits a reduced release efficiency at later times compared to the low-power condition. **(B)** Stress relaxation curve of hydrogels (λ = 3.0) under low- and high-power ultrasound. High-power ultrasound induces a pronounced stress decay over time, indicating polymer network damage and chain scission. Values in **A** represent mean ± SD ($n = 3$).

originate from direct ultrasound-induced fluorescence variation or sonochemical bleaching of the dye molecules. Instead, the result suggests that excessive ultrasound intensity alters the hydrogel matrix and thereby modifies the release behavior.

At higher acoustic intensities, additional nonlinear effects may emerge, including more pronounced oscillatory strain fields and possible cavitation-related microflows [12, 44, 45]. These effects can substantially amplify local stress concentrations within the polymer network, driving the material beyond a purely elastic or viscoelastic response and into a regime of irreversible structural alteration. As a result, transport is no longer governed solely by enhanced diffusion, but instead reflects a coupled process involving diffusion, advection, and progressive network disruption. In this regime, heterogeneous transport pathways may arise from bulk material damage. Polymer chain scission, microcrack formation, and local delamination within the hydrogel can temporarily redistribute particles within fractured regions, thereby reducing the effective outward flux into the surrounding bath. In addition, high-energy acoustic fields may promote particle aggregation or adsorption onto polymer debris and container surfaces, further decreasing the freely suspended particle concentration detected in solution. Together, these effects can produce a dynamic and spatially non-uniform release profile that deviates from classical Fickian behavior.

To further test whether high-power ultrasound alters the hydrogel structure, we performed independent mechanical measurements under different ultrasound conditions. The stress relaxation results provide initial support for this interpretation. As shown in Fig. 8B, the hydrogel subjected to high-power ultrasound (Output power = 8) exhibited a pronounced decrease in load-bearing capacity over time, consistent with progressive network softening and structural weakening. However, because stress relaxation under sustained deformation may also include contributions from reversible viscoelastic effects, this result alone does not unambiguously prove permanent network damage. We therefore further performed pure-shear tensile tests on hydrogel samples after defined ultrasound treatments using both unnotched and notched geometries (Fig. 9A, C, and D). Compared with the low-power condition (Output power = 4), hydrogels exposed to high-power ultrasound exhibited reduced shear modulus, elastic modulus, fracture stress, fracture strain, and fracture toughness (Fig. 9B), indicating a clear loss of network integrity after ultrasound treatment. These direct mechanical measurements support the conclusion that the reduction in load-bearing capacity under strong ultrasound is not solely attributable to reversible relaxation, but is instead consistent with permanent structural degradation of the hydrogel network.

Moreover, because the elastic modulus is directly related to the effective network density, the observed reduction in modulus also suggests a loosening of network constraint and an increase in effective mesh size, which is relevant to the diffusion behavior discussed in this work. It should also be noted that the acoustic wavelength is orders of magnitude larger than the hydrogel mesh size, indicating that ultrasound does not directly couple to nanoscale network heterogeneity at the molecular-mesh level. Instead, ultrasound is considered here as a bulk mechanical perturbation that induces transient fluctuations of the polymer matrix and embedded particles, thereby modulating the local transport energy landscape. Under low- and intermediate-power conditions, this perturbation enhances mechano-diffusion in a particle-size-dependent manner. Beyond a critical ultrasonic power threshold, however, the system

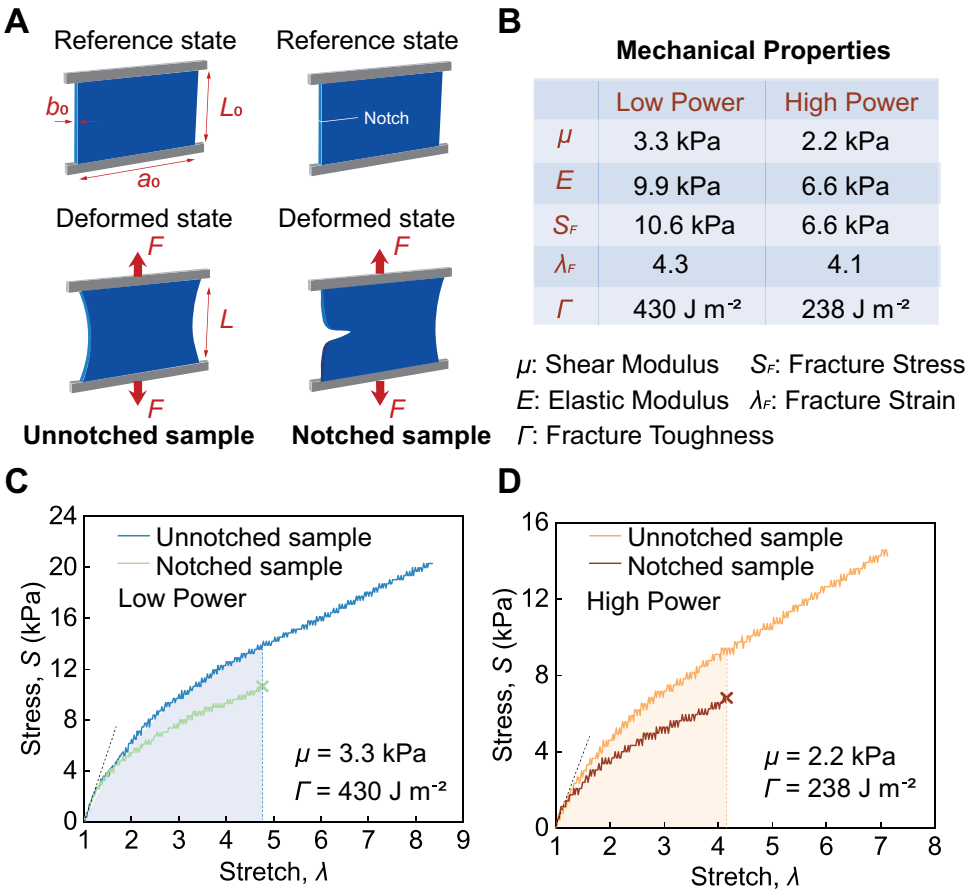


Fig. 9 Mechanical characterization of hydrogels after ultrasound treatment at different power levels. (**A**) Schematic illustration of pure shear tensile testing on unnotched and notched hydrogel samples in the reference and deformed states. **(B)** Summary of the mechanical properties of hydrogels following low-power (Output = 4) and high-power (Output = 8) ultrasonic treatments, including shear modulus μ, elastic modulus E, fracture stress S_F, fracture stretch λ_F, and fracture toughness Γ. **(C, D)** Stress–stretch curves from pure shear tensile tests, along with the fracture stretch of notched specimens and the corresponding fracture toughness, for hydrogels treated with low-power ultrasound (Output = 4) **(C)** and high-power ultrasound (Output = 8) **(D).**

appears to transition from a reversible mechano-diffusion regime to a damage-dominated transport regime.

Selectivity Enhanced by Ultrasound Stimulation

In the previous single-tracer release experiments, the concentration of FITC–dextran in the PBS bath was quantified using a fluorescence intensity analyzer, and the measured fluorescence signals were converted to solution concentrations using pre-established intensity–concentration calibration curves. For the subsequent selective-transport experiments, however, FITC–dextran (4 kDa) and Rhodamine B were simultaneously incorporated into the same hydrogel matrix. Under these conditions, single-wavelength fluorescence measurements are not ideal because partial spectral overlap and signal coupling between fluorophores can hinder independent quantification of each species. To overcome this limitation, we adopted UV–Vis absorption spectroscopy using a NanoDrop platform. As shown in Fig. 10A, the mixed solution exhibits two well-separated absorption peaks centered at approximately 490 nm and 550–560 nm, corresponding to FITC–dextran and Rhodamine B, respectively, thereby enabling independent signal extraction for each tracer. Within the tested concentration range, the absorbance at each characteristic wavelength increased systematically with concentration, allowing separate calibration relationships to be established for quantitative analysis. The concentration-dependent absorption spectra of Rhodamine B are shown in Fig. 10B over the range of 2–10 μM, and the corresponding calibration curve in Fig. 10C shows a strong linear relationship between absorbance and concentration with minimal experimental variation, supporting accurate back-calculation of tracer concentrations in the external PBS bath during release experiments. This measurement strategy therefore enables simultaneous and decoupled quantification of multiple tracers released from the same hydrogel system.

Rhodamine B was selected as the small-molecule tracer because its estimated hydrodynamic size is only on the order of ~1–2 nm, corresponding to $d/\xi \approx 0.06 - 0.13$ in the present hydrogel network ($\xi \approx 15.96$ nm). This places Rhodamine B well within the small-particle diffusion regime, where transport is only weakly constrained by the polymer network. To provide the most meaningful polymer-tracer comparison, we paired Rhodamine B with 4 kDa FITC–dextran, the smallest FITC–dextran species used in this study. Because Rhodamine B is still substantially smaller than any FITC–dextran tracer, this choice minimizes the size disparity

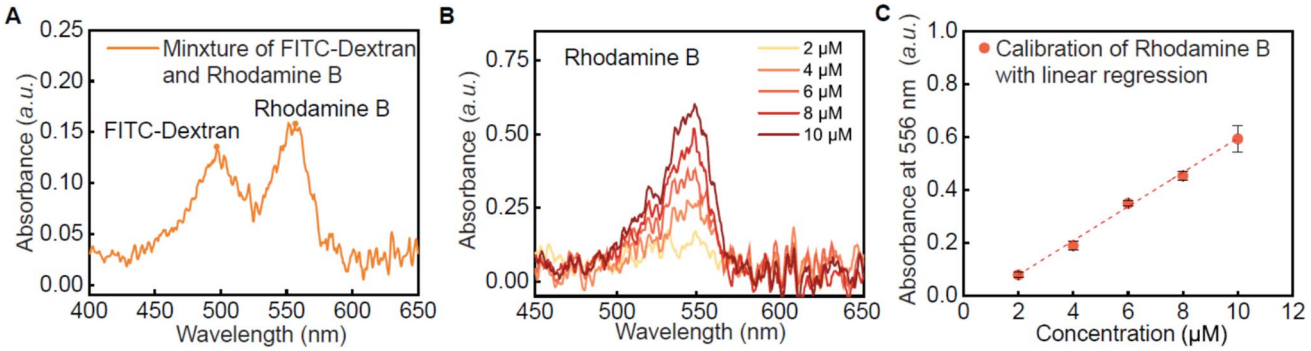


Fig. 10 Spectral characterization and calibration of Rhodamine B and FITC–dextran. (**A**) UV–Vis absorption spectrum of a mixed FITC–dextran and Rhodamine B solution, showing two distinct characteristic peaks at ~ 490 nm and ~ 556 nm. (**B**) Concentration-dependent absorption spectra of Rhodamine B over a range of concentrations. (**C**) Calibration curve of Rhodamine B obtained from absorbance values at 556 nm with linear regression fitting, enabling quantitative concentration determination in diffusion experiments. Values in **C** represent mean ± SD ($n = 3$).

within the FITC–dextran series while preserving the contrast between small-molecule transport and polymer-tracer transport. Together, this tracer pair provides a useful model system for evaluating ultrasound-mediated, size-dependent selective diffusion in the hydrogel network.

The central objective of this section is to evaluate how ultrasound and stretching influence selective release. To quantitatively compare the transport of the two tracers, effective diffusivities were extracted from the concentration–time relationships for Rhodamine B and 4 kDa FITC–dextran under each condition, and the corresponding selectivity was evaluated based on their diffusivity ratio as defined above.

Ultrasound-induced heating should also be considered when interpreting the observed selective transport behavior. Under the sonication conditions used in this study (output = 4, duty cycle = 40%), the PBS -bath temperature increased from approximately 20 °C to about 40–41 °C within the first 20 min and then remained nearly constant, indicating the establishment of a thermal steady state (Fig. 11A). This temperature rise may contribute to transport enhancement by reducing solvent viscosity and increasing diffusivity. In addition, the probe was positioned approximately 1 cm above the center of the hydrogel sample with the tip immersed in the water bath, and this configuration was kept constant across experiments to improve reproducibility. Because the acoustic field in such a probe-based setup is likely to be spatially non-uniform, both thermal effects and local acoustic heterogeneity should be taken into account when interpreting ultrasound-regulated selective transport.

To further examine whether the increase in selectivity could be attributed solely to ultrasound-induced heating, we performed additional control release experiments for

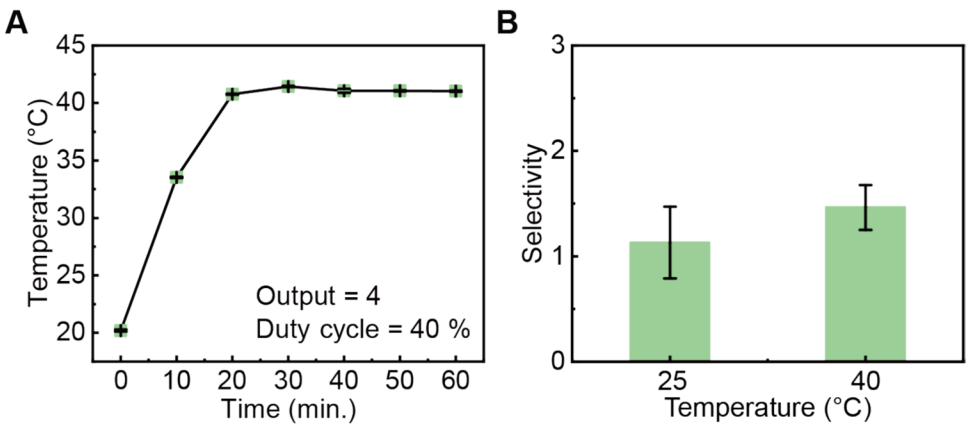


Fig. 11 Evaluation of ultrasound-associated thermal effects on hydrogel selectivity. (**A**) Time-dependent temperature evolution of the PBS bath under ultrasound stimulation (output = 4, duty cycle = 40%). (**B**) Comparison of particle release selectivity at room temperature (25 °C) and elevated temperature (40 °C), where both hydrogel samples were subjected to $\lambda = 2$ in the absence of ultrasound stimulation. The similar selectivity values observed at the two temperatures indicate that bulk heating alone cannot explain the ultrasound-enhanced selective transport behavior. Values represent mean ± SD ($n = 3$).

FITC–dextran and Rhodamine B in a hot PBS bath and compared the resulting selectivity (Fig. 11B). Under room-temperature conditions, the selectivity remained close to 1. When the PBS bath temperature was raised to 40 °C, the selectivity increased only modestly, from approximately 1 to about 1.5. This result confirms that thermal effects do influence the release of different molecules to some extent. However, the increase in selectivity caused by heating alone was relatively small and remained quantitatively much weaker than the selectivity enhancement observed under the combined action of ultrasound and stretching. Therefore, although the thermal contribution cannot be neglected, it is insufficient to account for the much larger selective-transport enhancement induced by ultrasound-assisted mechano-diffusion.

To evaluate how stretching and ultrasound influence selective release, the following experiments were divided into three groups using hydrogels co-loaded with Rhodamine B and 4 kDa FITC–dextran: stretching alone, ultrasound alone, and combined stretching with ultrasound. Representative release curves are shown in Fig. 12A–C. Under stretching-only and ultrasound-only conditions, the normalized concentration profiles of Rhodamine B and FITC–dextran exhibited broadly similar trends. Although direct comparison of the absolute release curves is not the primary objective of this experiment, several useful observations can still be drawn. In particular, for this tracer pair, stretching produced a stronger effect on release behavior than ultrasound alone, which is consistent with our earlier conclusion that ultrasound has only a limited influence on small-molecule transport.

By contrast, under the combined action of stretching and ultrasound (Fig. 12C), the release rate of Rhodamine B became clearly higher than that of FITC–dextran. This distinction was further confirmed by the fitted effective diffusivities and the resulting selectivity values. To summarize the combined influence of stretching and ultrasound on selective transport, a 3D plot is presented in Fig. 12D. It can be seen that ultrasound alone produced little enhancement in selectivity, and in some cases even resulted in selectivity values below 1, indicating that ultrasound affected the larger FITC–dextran tracer more strongly than the smaller Rhodamine B under those conditions. In comparison, stretching alone led to a modest increase in selectivity, typically in the range of 1–1.5. Notably, when ultrasound and stretching were applied simultaneously, the selectivity increased substantially, reaching values of approximately 1.5–3. These results indicate that the combined effect of ultrasound and stretching is non-additive, leading to a much greater increase in selectivity than either perturbation alone.

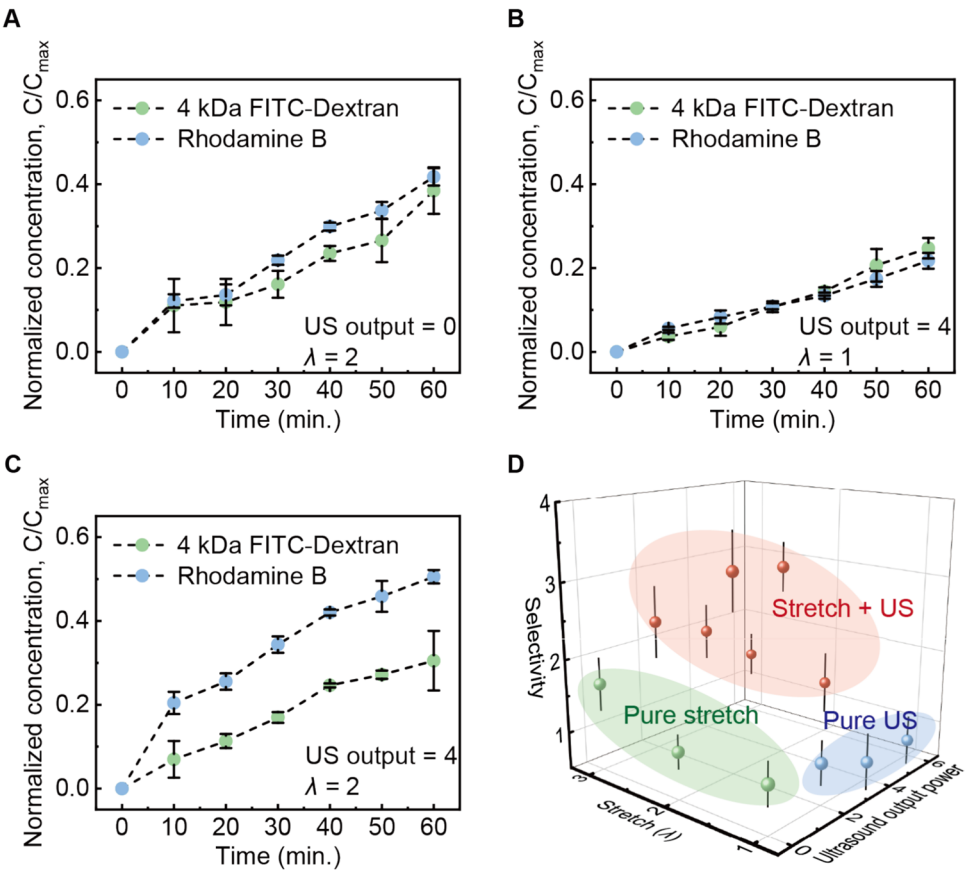


Fig. 12 Synergistic effect of mechanical stretching and ultrasound stimulation on selective particle release in hydrogels. Time-dependent normalized release profiles of Rhodamine B and 4 kDa FITC–dextran under (**A**) pure mechanical stretching, (**B**) pure ultrasound stimulation, and (**C**) the combined application of stretching and ultrasound. (**D**) Comparison of release selectivity under pure mechanical stretching, pure ultrasound stimulation, and their combined effect, demonstrating enhanced size-selective transport when mechanical deformation and ultrasonic stimulation are simultaneously applied. Values represent mean ± SD ($n = 3$).

Conclusions

In this work, we establish an ultrasound-mediated mechano-diffusion platform that enables dynamically programmable, size-selective particle transport in polymeric hydrogels, overcoming the challenge of achieving selective diffusion under nearly identical thermodynamic and kinetic conditions. Through the development of the ultrasound diffusion characterization platform (UDCP), we enable orthogonal control of mechanical deformation and acoustic energy input, allowing systematic decoupling of structural modulation from energy-driven transport enhancement. Mechanistically, particle transport is governed by the size relationship between the diffusing species and the network mesh. Ultrasound enhances transport by elevating particle kinetic activity and modulating dynamic fluctuations of the polymer network, thereby reshaping the effective energy landscape for barrier crossing, while mechanical stretching alters the baseline barrier level through structural reconfiguration. Because particles operating under distinct transport regimes respond differently to external stimulation, ultrasound induces non-uniform enhancement across different types of nanoparticles, amplifying pre-existing transport disparities and leading to enhanced selectivity. Importantly, ultrasound represents a non-contact and remotely controllable actuation strategy that enables volumetric energy delivery without requiring magnetic additives or embedded components. Compared with magnetic-field-based approaches, acoustic stimulation is directly compatible with chemically inert and structurally uniform hydrogel systems and provides continuously tunable dynamic control. Collectively, this study establishes a physically programmable framework for selective diffusion engineering, expanding the design space for targeted delivery, smart filtration, environmental remediation, and adaptive soft material systems.

Author Contributions Chuwei Ye: Conceptualization, Methodology, Investigation, Writing—original draft, Writing—review & editing. Tsz Hung Wong: Conceptualization, Methodology, Investigation, Supervision, Writing—original draft, Writing—review & editing. Yiwen Zheng: Methodology, Investigation. Ruihao Lu: Methodology, Investigation. Jie Ma: Methodology, Investigation, Writing—review & editing. Shaoting Lin: Conceptualization, Methodology, Supervision, Writing—review & editing.

Funding We acknowledge partial support from the donors of the American Chemical Society Petroleum Research Fund through grant PRF 69156-DNI9. This work was also supported by NSF-CBET-2320716 and NSF-CMMI-2338747.

Data Availability All data of this study are available from the corresponding author upon reasonable request.

Declarations

Competing interests The authors declare that they have no competing interests.

Open Access This article is licensed under a Creative Commons Attribution 4.0 International License, which permits use, sharing, adaptation, distribution and reproduction in any medium or format, as long as you give appropriate credit to the original author(s) and the source, provide a link to the Creative Commons licence, and indicate if changes were made. The images or other third party material in this article are included in the article's Creative Commons licence, unless indicated otherwise in a credit line to the material. If material is not included in the article's Creative Commons licence and your intended use is not permitted by statutory regulation or exceeds the permitted use, you will need to obtain permission directly from the copyright holder. To view a copy of this licence, visit http://creativecommons.org/licenses/by/4.0/.

References

1. Lieleg O, Ribbeck K (2011) Trends Cell Biol 21:543–551
2. Lee BJ, Cheema Y, Bader S, Duncan GA (2021) JCIS Open 4:100025
3. Al-Obaidi H, Florence AT (2015) Journal of Drug Delivery Science and Technology 30:266–277
4. Liu G, Zhong H, Ahmad Z, Yang X, Huo L (2020) Crit Rev Environ Sci Technol 50:2301–2378
5. Tungittiplakorn W, Lion LW, Cohen C, Kim J-Y (2004) Environ Sci Technol 38:1605–1610
6. Huang L, Zhang M, Li C, Shi G (2015) The journal of physical chemistry letters 6:2806–2815
7. Salafi T, Zeming KK, Zhang Y (2017) Lab Chip 17:11–33
8. Kuang X, Rong Q, Belal S, Vu T, López López AM, Wang N, Arıcan MO, Garciamendez-Mijares CE, Chen M, Yao J, Self-enhancing sono-inks enable deep-penetration acoustic volumetric printing, (2023) Science 382:1148–1155
9. Kuang X, Rong Q, Belal S, Wang N, Vu T, Herrera-Ruiz A, Zhang Z, Zhang YS, Yao J, Sonicated inks and focused-ultrasound writing enable deep-penetration acoustic volumetric printing, (2025) Nature Protocols 1–41
10. Davoodi E, Li J, Ma X, Najafabadi AH, Yoo J, Lu G, Sani ES, Lee S, Montazerian H, Kim G (2025) Science 388:616–623
11. Wang C, Chen X, Wang L, Makihata M, Liu H-C, Zhou T, Zhao X (2022) Science 377:517–523
12. Ma Z, Bourquard C, Gao Q, Jiang S, De Iure-Grimmel T, Huo R, Li X, He Z, Yang Z, Yang G (2022) Science 377:751–755
13. Wong TH, Liu W, Li J, Ma J, Cheng Y, Lu R, Koster KJ, Cirillo JD, Liu X and Sasaki H, Tissue-adhesive hydrogel–MXene biosensor for in situ intraoral TNF-α detection, (2026) Science Advances 12:eady9180
14. Wong TH, Liu J, Cheng Y, Xie Y, Anway C, Lu R, Ye C, Yu Z, Wang Y, Liu X (2025) Advanced Intelligent Systems 7:2400697
15. Tian Y, Yang Y, Wang J, Li N, Pan Z, Li Y, Zhou M, Huang Y, Zhang X, Yu Y (2025) Nat Commun 16:7910
16. Liu X, Tang H, Li N, He L, Tian Y, Hao B, Xue J, Yang C, Sung JJY, Zhang L, Miniature magneto-ultrasonic machines for wireless robotic sensing and manipulation, (2025) Science Robotics 10:eadu4851
17. Ilie F (2018) Int J Heat Mass Transf 116:1260–1265
18. Gorshkov V, Zavalov A, Privman V (2009) Langmuir 25:7940–7953
19. Adamczyk Z (2000) J Colloid Interface Sci 229:477–489
20. Dunsing V, Irmscher T, Barbirz S, Chiantia S (2019) Biomacromol 20:3842–3854
21. Goodrich CP, Brenner MP, Ribbeck K (2018) Nat Commun 9:4348
22. Sadeghi I, Kaner P, Asatekin A (2018) Chem Mater 30:7328–7354

23. Park HB, Kamcev J, Robeson LM, Elimelech M, Freeman BD,Maximizing the right stuff: The trade-off between membrane permeability and selectivity, (2017) Science 356:eaab0530
24. Nicolella P, Lauxen D, Ahmadi M, Seiffert S (2021) Macromol Chem Phys 222:2100076
25. Gu Y, Distler ME, Cheng HF, Huang C, Mirkin CA (2021) J Am Chem Soc 143:17200–17208
26. Hu Q-D, Tang G-P, Chu PK (2014) Acc Chem Res 47:2017–2025
27. Gyanani V, Goswami R (2023) Pharmaceutics 15:1184
28. Ye C, Wei C, Liu J, Wong TH, Liu X, Song Z, Wu C, Li Z, Lin S (2025) Soft Matter 21:2230–2241
29. Liu J, Lin S (2024) J Mech Phys Solids 191:105732
30. Ye C, Lin S (2024) MRS Communications 14:919–926
31. Venkatadri TK, Ye C, Cohen T, Lin S (2025) J Mech Phys Solids 198:106064
32. Karki A, Marshall JS, Wu J (2022) The Journal of the Acoustical Society of America 152:640–650
33. Qiu W, Bruus H, Augustsson P (2020) Phys Rev E 102:013108
34. Wang T, Ke M, Qiu C, Liu Z (2016) Journal of Applied Physics 119
35. Giri A, Walton SG, Tomko J, Bhatt N, Johnson MJ, Boris DR, Lu G, Caldwell JD, Prezhdo OV, Hopkins PE (2023) ACS Nano 17:14253–14282
36. Mizrahi N, Zhou EH, Lenormand G, Krishnan R, Weihs D, Butler JP, Weitz DA, Fredberg JJ, Kimmel E (2012) Soft Matter 8:2438–2443
37. Mares JO, Miller J, Gunduz I, Rhoads J, Son SF (2014) Journal of Applied Physics 116
38. Tartakovsky DM, Dentz M (2019) Transp Porous Media 130:105–127
39. Chen J, Chen Y, Li H, Lai S-Y, Jow J (2010) Ultrason Sonochem 17:66–71
40. Rubinstein M, Colby RH (2003) Polymer physics. Oxford university press
41. Amsden BG (2022) Macromolecules 55:8399–8408
42. Siepmann J, Peppas NA (2011) Int J Pharm 418:6–12
43. Crank J (1979) The mathematics of diffusion. Oxford university press
44. Yang J, McGhee A, Tong Z, Bu L, Wang S, Radtke G, Rodriguez M, Franck C (2026) Computer Vision & Laser Vibrometry, vol Vol. 6. River Publishers, pp 1–12
45. Tzoumaka A, Yang J, Buyukozturk S, Franck C, Henann DL (2023) Soft Matter 19:3895–3909

Publisher's Note Springer Nature remains neutral with regard to jurisdictional claims in published maps and institutional affiliations.